ACS OMEGA

http://pubs.acs.org/journal/acsodf

Article

Insight into Cellular Uptake and Transcytosis of Peptide Nanoparticles in *Spodoptera frugiperda* Cells and Isolated Midgut

Erin McGraw,[†] Jonathan D. Roberts,[†] Nitish Kunte, Matthew Westerfield, Xavier Streety, David Held, and L. Adriana Avila*

Cite This: *ACS Omega* 2022, 7, 10933−10943

Read Online

ACCESS | Metrics & More | Article Recommendations | Supporting Information

ABSTRACT: Silencing genes in insects by introducing double-stranded RNA (dsRNA) in the diet holds promise as a new pest management method. It has been demonstrated that nanoparticles (NPs) can potentiate dsRNA silencing effects by promoting cellular internalization and protecting dsRNA against early degradation. However, many mysteries of how NPs and dsRNA are internalized by gut epithelial cells and, subsequently, transported across the midgut epithelium remain to be unraveled. The sole purpose of the current study is to investigate the role of endocytosis and transcytosis in the transport of branched amphipathic peptide nanocapsules (BAPCs) associated with dsRNA through midgut epithelium cells. *Spodoptera frugiperda* midguts and the epithelial cell line Sf9, derived from *S. frugiperda*, were used to study transcytosis and endocytosis, respectively. Results suggest that clathrin-mediated endocytosis and macropinocytosis are largely responsible for cellular uptake, and once within the midgut, transcytosis is involved in shuttling BAPCs−dsRNA from the lumen to the hemolymph. In addition, BAPCs were not found to be toxic to Sf9 cells or generate damaging reactive species once internalized.

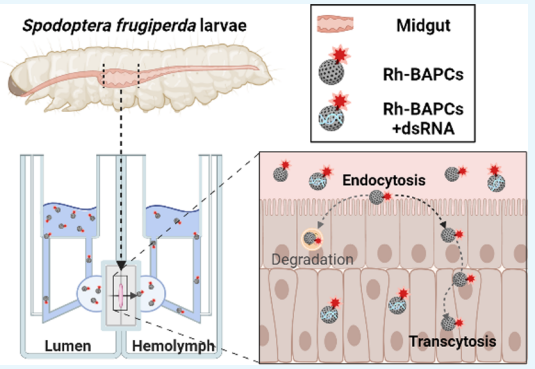

1. INTRODUCTION

Nanoparticle (NP)-mediated double-stranded RNA (dsRNA) delivery through feeding has become a promising approach for sustainable pest management.[1,2] Cellular processing of dsRNA causes the silencing of vital genes, thus resulting in selective killing of targeted insect species.[3] Association of dsRNA with NPs protects the dsRNA from nucleases, harsh gut environment conditions, and also promotes translocation of dsRNA across the cell membrane.[2] Hence, NPs are able to enhance the silencing effects triggered by dsRNA. However, specifics of how nanoparticle−dsRNA complexes are internalized by gut cells and their subsequent path through the midgut tissue remains a mystery.

Our research team developed peptide NPs called branched amphipathic peptide capsules (BAPCs).[4] These unique peptide nanovesicles, or peptosomes, have been used successfully as delivery system of dsRNA and DNA in a variety of cell lines, including insect cells.[2,5,6] BAPCs form through the spontaneous assembly of two branched amphipathic peptides, bis(Ac-FLIVI)$_2$−K−K$_4$−CONH$_2$ and bis(Ac-FLIVIGSII)$_2$−K−K$_4$−CONH$_2$, in water. The association of BAPCs with nucleic acids, such as dsRNA, occurs mainly through electrostatic interactions between the cationic ε-amino groups on the polylysine tails and the anionic phosphates on the dsRNA backbone.[7]

Our published studies demonstrated that feeding dsRNA−BAPCs complexes successfully targeted essential genes in the red flour beetle (*Tribolium castaneum*) and the pea aphid (*Acyrthosiphon pisum*), leading to high mortality rates.[6] In both species, BiP and Armet, genes involved in the unfolded protein response (UPR) were suppressed, resulting in lethality.[8,9] For *A. pisum*, ingestion of <10 ng of BiP−dsRNA associated with BAPCs led to the premature death of 75% of the subjects (n = 60) by day 5. The life span of *A. pisum* adult is about 20−30 days. *T. castaneum* larvae were effectively killed by ingestion using a combination of BiP−dsRNA and Armet−dsRNA complexed with BAPCs. By day 40, 75% of the subjects (n = 30) died as larvae or during eclosion. The life span of *T. castaneum* adult is around 2 years. Food supplemented exclusively with BAPCs did not affect survival rates. These results confirmed that complexation of dsRNA with BAPCs enhanced the oral delivery of dsRNA over dsRNA alone.[6]

The sole purpose of the present article is to gain insight into the cellular uptake mechanisms, endosomal escape, cytotox-

Received: November 23, 2021
Accepted: February 28, 2022
Published: March 22, 2022

icity, and transport across the insect midgut epithelium of the dsRNA−BAPC complexes. As reported previously, BAPC−dsRNA complexes were able to cause knockdown in the *T. castaneum* vermillion gene that encodes a protein required for the development of normal eye color.[6,10] Generally, effects of dsRNA are restricted to the delivery location (gut epithelium), but the absence of vermillion transcripts proved the ability of BAPC−dsRNA complexes to target genes outside of the gut.[11] To elucidate if transcytosis (a special type of vesicle-mediated transport) was involved in the translocation of the dsRNA−BAPC complexes through insect midguts, we mimicked ingestion of BAPCs in sixth instar *Spodoptera frugiperda* larvae. Isolated midgut tissues were carefully mounted into an Ussing chamber, along with biological buffers and rhodamine-labeled BAPCs (Rh−BAPCs).[12] Ussing chambers utilize special buffers that mimic in vivo conditions and are divided into chambers separated by the harvested midgut tissue to create an ex vivo setting that allows for the study of BAPC transcytosis.[13] Our findings indicated that transcytosis is involved in the transport of BAPCs and dsRNA−BAPC complexes across *S. frugiperda* midgut tissue.

Additionally, we explored the specific endocytic routes involved in the cellular internalization of BAPCs with and without dsRNA in the Sf9 cell line.[14] Cellular internalization processes can be broadly classified as clathrin-dependent or clathrin-independent. The clathrin-independent pathways can be more specifically classified as caveolae-dependent endocytosis, clathrin- and caveolae-independent endocytosis, and macropinocytosis.[15] To date, the best documented endocytic pathway in insects is the clathrin-dependent pathway.[16,17] Although endocytosis of dsRNA associated with nanoparticles has been studied extensively in mammalian cells, details of those particular pathways in insect cells remains largely unknown.[17,18] To probe the dependency of BAPC nanoparticles on different endocytic routes, we exposed Sf9 cells to BAPCs or BAPC−dsRNA complexes in the presence of selective endocytic inhibitors.[19] Confocal analysis demonstrated that clathrin-dependent endocytosis and macropinocytosis are the predominant uptake pathways used by BAPC−dsRNA complexes to access the cytosol of Sf9 cells.

Lysosome colocalization experiments were also performed to evaluate the fraction of BAPC−dsRNA complexes trapped within this degradative organelle. Increased presence of complexes within lysosomes may result in degradation of the dsRNA, thus reducing possible systemic delivery of dsRNA and silencing effects.[20] Results show that BAPCs only minimally colocalize within lysosomes. Production of reactive oxygen (ROS) and nitric oxide (NOS) species was also analyzed to ensure that the BAPC−dsRNA complexes did not generate oxidative stress in cells, which could affect off-target species. No significant production of ROS or NOS was found when Sf9 cells were exposed to BAPCs or BAPC−dsRNA complexes.

2. RESULTS AND DISCUSSION

2.1. Biophysical Characterization of BAPC−dsRNA Complexes. In this section, we sought to analyze the size and shape of the BAPCs associated with a 252 bp dsRNA (CYP-450). Transmission electron microscopy (TEM) analysis revealed that, similar to previous atomic force microscopy (AFM) studies performed with a 390 bp dsRNA (BiP), BAPCs can act as cationic nucleation centers around which the negatively charged phosphate backbone winds, generating BAPC−dsRNA complexes with sizes ranging from 50 to 250 nm (Figure 1A−C).[5,6] Formation of these complexes aids in

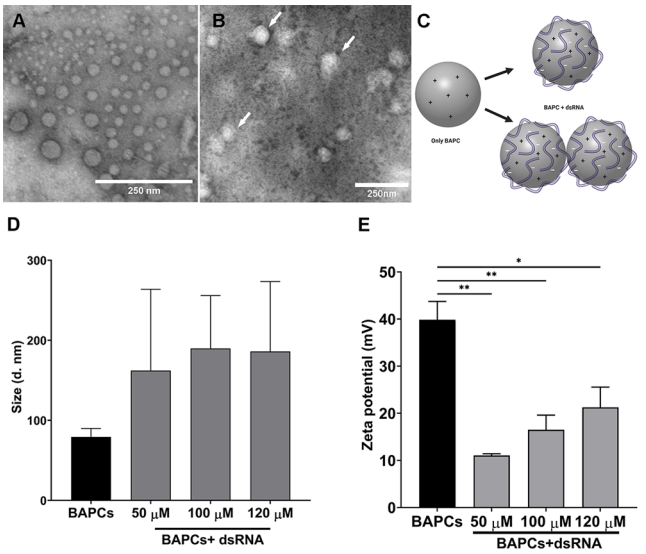

Figure 1. Biophysical characterization of BAPCs and BAPC−dsRNA complexes. (A) TEM analysis of bare BAPCs (50 μM) and (B) TEM analysis of BAPCs (50 μM) associated with dsRNA (1 μg). (C) Schematic representation of the BAPC−dsRNA complexes. (D) DLS and (E) ZP analysis of BAPC−dsRNA complexes at different concentrations associated with dsRNA (1 μg) . Statistical significance: (*) $p < 0.033$; (***) $p < 0.001$; (ns) $p > 0.12$ versus 50 μM BAPCs without dsRNA.(ANOVA, Tukey posttest).

protecting dsRNA against nucleases. The electrostatic association of dsRNA with BAPCs hinders nuclease binding sites, as we confirmed experimentally in previous studies.[21] The tangible silencing effects observed on *T. castaneum* and *A. pisum* also supports the protective role provided by BAPCs against nucleases and other potential degradation agents in the insect gut.[6]

To further expand the biophysical analysis of the BAPC−dsRNA complexes, we also performed a DLS analysis.[22] This technique is used to determine the hydrodynamic diameter of nanoparticles dispersed in a liquid medium by measuring changes in the intensity of the scattered light.[17] The hydrodynamic diameter will depend not only on the size of the particle "core" but also ions present on the surface. In general, particles with a larger hydrodynamic diameter scatter much more light than small particles.[23] Different BAPCs and dsRNA formulations were analyzed by DLS by keeping the amount of dsRNA constant (1 μg) and varying the BAPCs concentration (Figures 1D and S1). The BAPCs−dsRNA complexes displayed larger hydrodynamic diameters than the bare BAPCs, suggesting the association of dsRNA increases the size of the BAPCs or causes BAPCs to cluster together, which agrees with the TEM results. Additionally, the increase in size after association with dsRNA also indicates that the complexes are tightly bound as they do not readily dissociate upon dilution.

Finally, we analyzed the zeta potential (ZP) of BAPCs and the BAPC−dsRNA complexes (Figure 1E). ZP is a measure of the magnitude of the electrostatic charge or repulsion/attraction between particles and is one of the fundamental parameters known to affect stability.[24] Positive ZP values might enhance electrostatic interactions with the negatively

https://doi.org/10.1021/acsomega.1c06638
ACS Omega 2022, 7, 10933−10943

charged cell membranes.[5,19] However, values above 45 mV can trigger high levels of toxicity.[25,26] To investigate the ZP values of BAPCs and the BAPC−dsRNA complexes, different concentrations of BAPCs were analyzed both alone and complexed with 1 μg of dsRNA. BAPCs showed ZP values of ∼40 mV, and this value decreased to ∼10−20 mV after association with dsRNA, confirming TEM analysis results that the dsRNA surrounds the peptide nanocapsules, thus altering the surface charge. Despite varying BAPC concentrations, the overall surface charge of the BAPC−dsRNA complexes remained positive, which facilitates interaction with negatively charged cell membranes.

2.2. Cellular Uptake Mechanisms and Lysosome Colocalization of BAPCs and BAPC−dsRNA complexes. Studies conducted in mouse macrophages and rat intestinal epithelial cells demonstrated that macropinocytosis, clathrin-, and caveolae-dependent endocytosis are the prominent endocytic modalities for BAPC internalization in animal cells.[27] In this article, we seek to elucidate the internalization pathway of BAPCs and the BAPC−dsRNA complexes in insect cells. To accomplish this goal, we incubated Sf9 cells with fluorescent labeled BAPCs (Rh−BAPCs) in the presence of selective endocytic inhibitors.[28] Subsequently, cellular internalization was monitored qualitatively using confocal microscopy.

To inhibit clathrin-mediated endocytosis, we used CPZ and dynasore. Dynasore inhibits dynamin, and CPZ sequesters adaptor proteins and clathrin, thus depleting it from the plasma membrane.[29,30] M-β-CD and nystatin were used to inhibit caveolae-dependent endocytosis.[29] M-β-CD and nystatin inhibit caveolae-dependent endocytosis by binding plasma membrane cholesterol which in turn perturbs fluidity of lipid rafts.[29,30] To prevent macropinocytosis, we treated cells with cytochalasin D, which is specifically inhibits macropinocytosis and phagocytosis by inducing depolymerization of actin filaments which are essential for coating the macropinosomes.[31] A list of all inhibitors used and their mode of action is listed in Table 1.

Table 1. Inhibitors Used to Study the Internalization and Transport of BAPCs

pathway	inhibitor	mode of inhibition	ref
clathrin-mediated	chlorpormazine	sequesters clathrin and AP2 from the cell membrane	29, 30
	dynasore	inhibits dynamin and acin polymerization	29, 30
caveolae-mediated	methyl-β-cyclodextrin	extracts cholesterol from plasma membrane	30
	nystatin	extracts cholesterol from plasma membrane	30
macropinocytosis	cytochalasin D	caps and prevents assembly of actin	29−31

Our results indicate that clathrin-mediated and macropinocytosis are the major endocytic routes employed by BAPCs to access the cytosol of Sf9 cells (Figures 2 and S2). Notably, for the BAPC−dsRNA complexes, the caveolae/lipid raft dependent endocytosis seemed to also play a role in the cellular internalization process. Several nanomaterials that have shown successful delivery use macropinocytosis since it forms a large leaky vesicle that can enclose several nanoparticles.[32] Therefore, it was expected that this pathway was involved in the uptake of BAPCs in Sf9 cells. Review of literature suggests that one cell type can endocytose the same nanoparticle using multiple pathways, as nanoparticle formulations are often made up of a group of heterogeneous particles with different sizes, which makes the uptake process more diverse.[33] Clathrin-mediated endocytosis, macropinocytosis, and caveolin-mediated endocytosis have been documented before in insect cells, including Sf9 cells for the uptake of dsRNA, viruses, proteins and lipoproteins.[34−38] Nonetheless, this is the first study that demonstrates the implication of these pathways in the internalization of dsRNA and dsRNA associated with peptide nanoparticles.

After cellular entry, internalized nanoparticles are delivered to the early endosome. Subsequently, the early endosomes undergo a maturation process that ultimately results in the formation of the endolysosome, a temporary hybrid organelle resulting from fusion of late endosomes and lysosomes (Figure 3A).[18] Lysosomes are regularly the final destination for external macromolecules and nanoparticles.[39] The lysosomal lumen has an acidic pH close to 4.5 and contains approximately 60 different soluble hydrolytic enzymes; thus, macromolecules and nanoparticles trapped within these organelles are often degraded.[40] Success in gene silencing through dsRNA is often hindered by the entrapment and subsequent degradation within this acidic organelle. This degradation process contributes to what is known as dsRNA resistance, and it has been a barrier for the development of broader applications of dsRNA-based technology in insects.[17]

To evaluate the entrapment of the BAPC−dsRNA complexes within the lysosomes; Rh−BAPCs complexed with dsRNA were incubated with Sf9 cells for 1 h, then lysosomes were stained using Cell Navigator. As shown in Figure 3, Rh−BAPC−dsRNA complex (Figure 3B) and the stained lysosomes (Figure 3C) are visualized in the Sf9 cells. Upon merging with bright field (Figure 3D), the two images show only a small fraction of the labeled BAPCs−dsRNA appeared to be colocalized within the lysosome, appearing as yellow spots indicated by white arrows (Figure 3E). These results suggest that BAPC−dsRNA complexes are processed by the endosomal route, yet rapidly escape the early or late endosomes. Most likely, the poly(L-lysine) tails of BAPC peptides trigger the rupture of the endosomes by osmotic pressure caused by a "proton sponge effect".[41]

The proton sponge effect is a proposed mechanism for nanoparticle endosomal escape.[42−44] In the case of BAPCs, the amine groups in the lysine tails act as proton sponges in acidic environments, thus creating a buffering system.[45] Protonation of the peptide causes an increase in pH, which in turn triggers an influx of protons in attempt to restore the acidic pH. Subsequently, water and other ions, such as chloride flood the vesicles, resulting in osmotic swelling. Osmotic swelling and pressure from electrostatic repulsions between similarly charged ions ultimately results in rupture of the lysosomal membrane. Once ruptured, the complexes are released into the cytosol, thus avoiding lysosomal entrapment and degradation—a previously identified source of failure of dsRNA in lepidopterans.[40,46] Future studies in the escape of BAPC−dsRNA complexes will include the modification of the peptide sequences to include histidine residues, which exhibit increased proton sponge effects.[47] Similarly to lysine amine groups, the histidine imidazole ring prevents endosome acidification by capturing protons. This in turn triggers ATPase proton pumps to continue to transport protons into the endosome, followed by the influx of water and ions, ultimately resulting in rupture.[1]

https://doi.org/10.1021/acsomega.1c06638
ACS Omega 2022, 7, 10933−10943

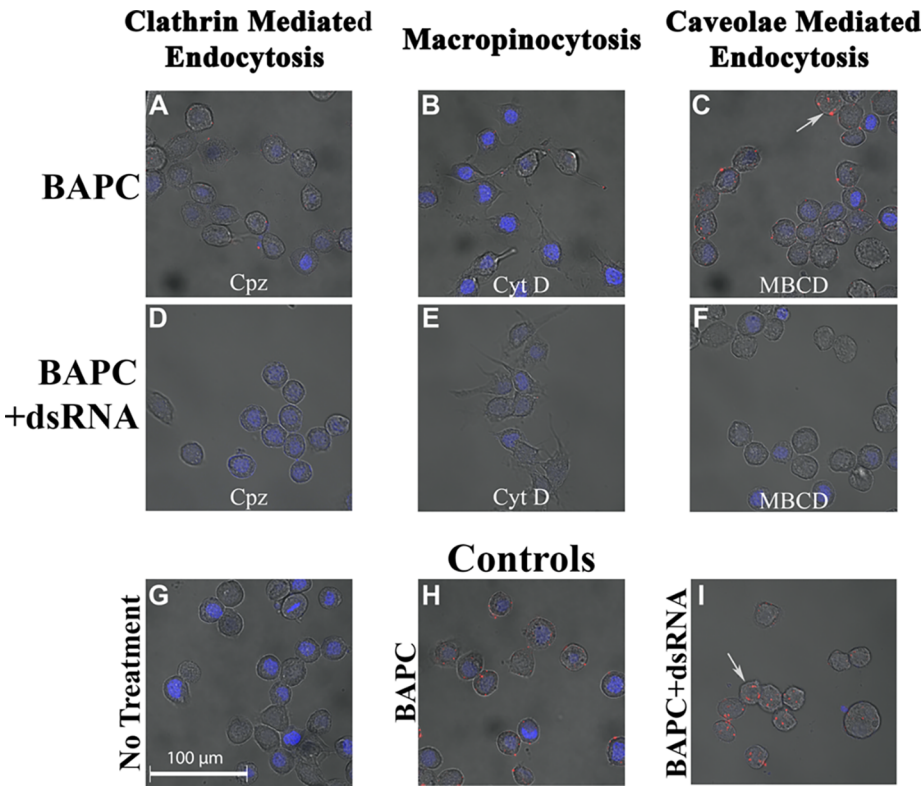

Figure 2. Endocytosis inhibition assay of BAPC and BAPC−dsRNA complexes in Sf9 cells. BAPCs were labeled with rhodamine B (red). Panels A−C correspond to uptake of BAPCs in the presence of inhibitors. Panels D−F correspond to uptake of BAPC−dsRNA complexes in the presence of inhibitors. Panel G are untreated Sf9 cells, and panels H and I are cells treated with BAPCs and BAPC−dsRNA complexes but without inhibitors.

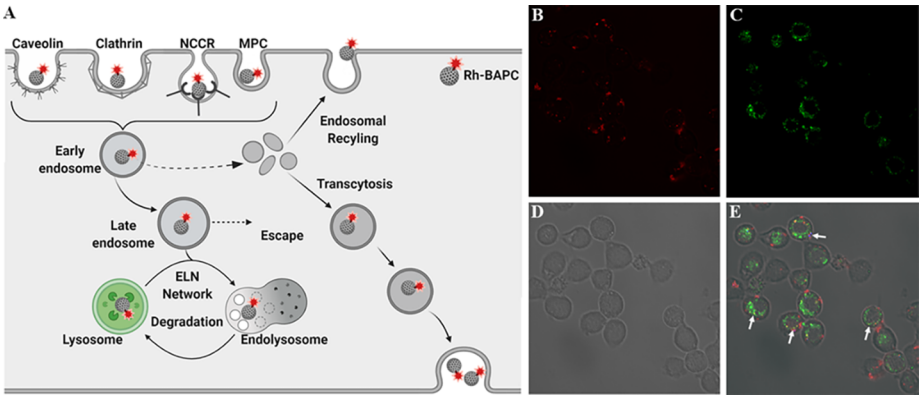

Figure 3. Colocalization of BAPCs with dsRNA in lysosomes. 2.5 μg of dsRNA was complexed with 50 μM of BAPCs and incubated with Sf9 cells for 1 h. Lysosomes were stained with Cell Navigator. Confocal microscopy was used to check for colocalization of complexes in lysosomes. (A) Schematic representation of endocytic pathways and endosome maturation process. (B) Rh−BAPCs (red), (C) lysosomes (green), (D) bright field, and (E) merge image showing colocalization of BAPCs and the lysosomes (yellow).

2.3. BAPC−dsRNA Uptake and Transport Across the Midgut Epithelium. Silencing effects in insects induced by ingestion of dsRNA are generally localized in the delivery site (midgut cells), thus effects are transient and gene targets limited. Systemic delivery is more desirable since allows targeting genes from the whole insect (not just gut-specific).[11] A better understanding of how these macromolecules cross the insect midgut will help to improve the oral delivery of dsRNA-based insecticides.[2] In some insect species, SID-1 like (SIL) channel proteins play a role in the uptake and midgut translocation of dsRNA.[48−51] However, these channel proteins are not present in all insect species, implying that alternative transport mechanisms contribute to the translocation of dsRNA and NPs through the gut. Transcytosis is an active trans-cell transportation process used by multicellular organisms to selectively move material between two environments without altering the unique compositions of those environments.[52] In animal cells, it was discovered that NPs are transported across biological barriers, such as the blood−brain barrier (BBB) through transcytosis.[52] In insects, the ability of viruses to transcytose across the gut epithelium and infect cells within the insect hemocoel has been well studied.[12]

To elucidate if transcytosis was involved in the translocation of BAPCs through midgut epithelium cells, midguts of sixth

https://doi.org/10.1021/acsomega.1c06638
ACS Omega 2022, 7, 10933−10943

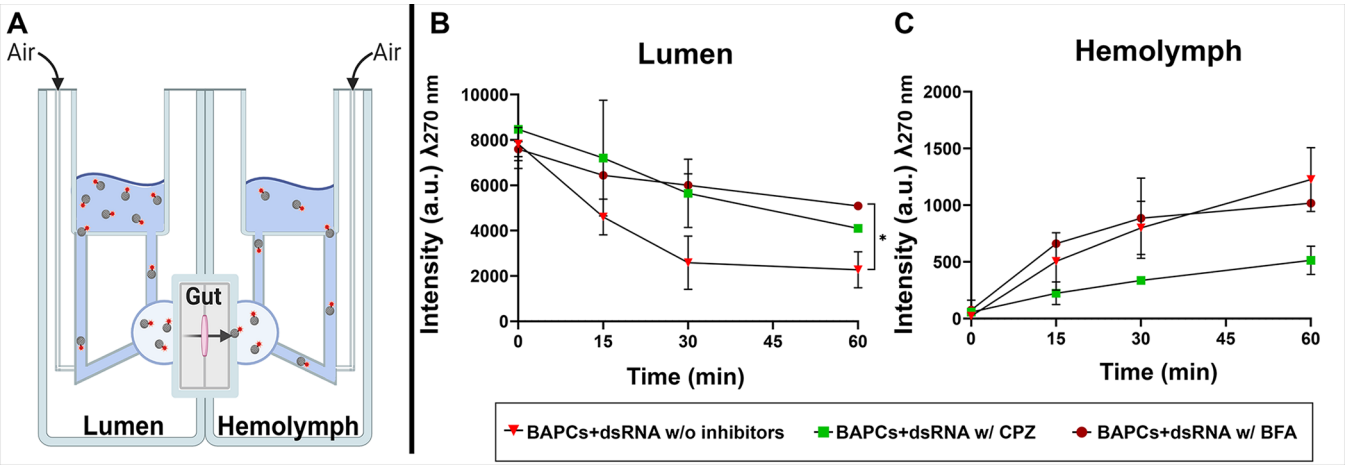

Figure 4. Transcytosis of Rh−BAPCs through *S. frugiperda* midgut in the presence of transcytosis and endocytosis inhibitors. (A) Scheme showing the movement of material through midgut tissue in an Ussing chamber. (B) Relative fluorescence of lumenal buffer or (C) hemolymph buffer over 1 h. Data represent mean values + SD of two experiments combined. Statistical significance: (*) $p < 0.033$; (***) $p < 0.001$; (ns) $p > 0.12$ versus Rh−BAPC + dsRNA control (no inhibitors) (ANOVA, Dunnett posttest).

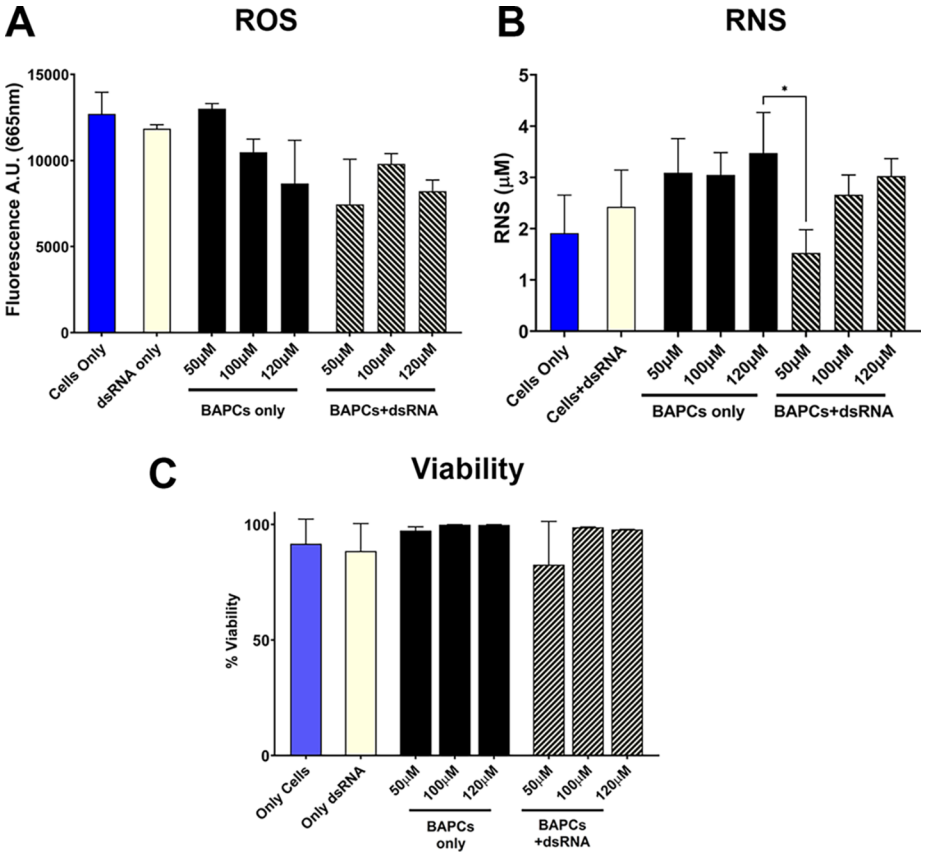

Figure 5. Effect of BAPC−dsRNA complexes on cell viability and oxidative stress. (A) Relative production of ROS based on treatment group. (B) Relative production of RNS based on treatment group. (C) How cell membrane integrity is affected by the different treatment groups using the dead cell exclusion dye 7-AAD. Data represent mean values + SD of two experiments combined. Statistical significance: (*) $p < 0.033$; (***) $p < 0.001$; (ns) $p > 0.12$ versus groups indicated in the bars (ANOVA, Dunnett posttest).

instar *S. frugiperda* larvae were exposed to Rh−BAPCs and Rh−BAPC−dsRNA complexes for over a period of 60 min in an Ussing chamber (Figure 4A). *S. frugiperda* was selected as a model due to the previously reported occurrence of viral transcytosis and the availability of adherent epithelial cell lines (Sf21 and Sf9) to provide comparable in vitro data.[12,53] Brefeldin-A (BFA) was used to study the potential role of transcytosis from the midgut lumen to the hemolymph. BFA is a selective transcytosis inhibitor that impacts the regulation and creation of Golgi transport vesicles.[54] Rh−BAPCs in the absence of BFA showed evident transcytosis (Figure S3). Nanoparticles were added into the lumenal side, and over time, Rh−BAPC moved into the hemolymph compartment, thus increasing the relative fluorescence of that compartment. If

https://doi.org/10.1021/acsomega.1c06638
ACS Omega 2022, 7, 10933−10943

active transport was not involved, the nanoparticles would have either remained within the tissue, thus causing no increase to the relative fluorescence of the hemolymph buffer, or diffusion of the buffers would have resulted in an equilibrium of fluorescence in both compartments. The relative fluorescence seen in the hemolymph increased after a period of 1 h, supports the occurrence of transcytosis (Figure 4C). Transcytosis of Rh−BAPCs associated with dsRNA showed a similar luminal uptake pattern. Nonetheless, the relative fluorescence detected in the hemolymph compartment was only slightly affected by the BFA inhibitor, suggesting that in the presence of dsRNA, alternative intracellular transport pathways are present. (Figures 4B and C and S3).

To explore the involvement of clathrin in transcytosis, we also exposed midgut tissues to the inhibitor chlorpromazine (CPZ), which affects the assembly and disassembly of the clathrin lattice found on clathrin-coated pits.[55] The availability of clathrin to form lattices around vesicles is required for both clathrin-mediated endocytosis and transcytosis.[56] According to Figure 4B, the addition of CPZ did reduce the degree of Rh−BAPC−dsRNA complex uptake from the lumen, thus resulting in much lower fluorescence in the hemolymph (Figure 4C). This has two implications: (1) the inhibition of clathrin-mediated endocytosis reduces transcytosis since there are fewer BAPC−dsRNA complexes available to traffic across the cell and (2) BAPC−dsRNA complexes internalized via macropinocytosis (alternative uptake route for BAPCs) are unable to be transported through the epithelium access the hemolymph.

2.4. Cytotoxicity of BAPCs and BAPC−dsRNA Complexes in Insect Cells. To ensure potential field applications of dsRNA-based technology, it is essential to understand the potential cytotoxic effects of the peptide nanoparticles and dsRNA in nontarget organisms. By using Sf9 cells and the nonspecific dsRNA targeting *P. japonica*, we evaluated the generation of reactive oxygen species (ROS) by cells in response to BAPCs and BAPC−dsRNA complexes. Production of ROS is a potent early marker for nanoparticle toxicity.[57,58] Although ROS toxicity is more commonly observed with metallic nanoparticles, measuring ROS production resulting from BAPC delivery in Sf9 cells gives us a better picture of potential downstream effects from a cytotoxicity perspective. One key factor involved in nanoparticle-induced ROS is the presence of prooxidant functional groups on the reactive surface of nanoparticles.[57] Production of ROS can disrupt mitochondrial activity, cause damage to DNA, and cause lipid peroxidation. This in turn destabilizes the cell membrane, making it more susceptible to oxidation.[59] ROS was detected using the CellROX Deep Red fluorescence assay.[60] The membrane permeable CellROX reagent is nonfluorescent until oxidized, and release of reactive oxygen species causes fluorescence at a maxima of 665 nm. According with the results (Figure 5A), BAPCs and the BAPC−dsRNA complexes did not cause a significant increase in the ROS when compared with untreated cells.

Similar to ROS, reactive nitrogen species (RNS) are naturally occurring within living systems. At low levels they are used by organisms for signaling purposes.[61] However, higher levels of RNS can be detrimental to the cells ultimately leading to cell death. In the instance that ROS and RNS production are both increased, there becomes the danger of creating peroxinitrite, which is a potent oxidative agent that can damage DNA.[61,62] The production of RNS in Sf9 cells was quantified using Griess Reagent alongside a standard curve. As show in Figure 5B, there is no significant difference between the control groups (untreated cells) and both BAPCs and BAPC−dsRNA complexes.

Cytotoxicity was evaluated by flow cytometry as well (Figure 5C). This is a rapid and reliable method commonly used to quantify cell viability.[63] Dead cells can be identified by using fluorescence probes that intercalate into DNA of cells with compromised cell membrane, such as 7-aminoactinomycin D (7-AAD). The viability of Sf9 cells treated with 50, 100, and 120 mM of BAPCs with or without dsRNA was minimally affected (<15% cell mortality), but according with the statistical analysis ($p > 0.12$), no significant difference was found when compared with untreated cells. We also analyzed viability in the presence of the endocytosis inhibitors, to ensure that this cell viability was preserved during the treatments. None of the inhibitors caused a decrease in cell viability or increase of oxidative stress, thus avoiding false-positive uptake results produced by damaged cell membranes (Figure S4). Altogether these results indicate that BAPCs neither induce cell death nor oxidative stress in insect cells. Moreover, studies conducted in mammalian cell lines and animal models also indicated that BAPCs do not induce acute toxicity and are not immunogenic, making them a suitable candidate for field applications for dsRNA delivery.[5]

3. CONCLUSIONS

The present study demonstrated that BAPCs and BAPC−dsRNA complexes are able to transverse the gut of *S. frugiperda* via an active transport process called transcytosis. Using a physiological chamber that mimics in vivo conditions, midguts of sixth instar *S. frugiperda* larvae were exposed to fluorescent BAPC complexes. Over an hour, fluorescence levels decreased in the lumenal compartment and increased in the hemolymph in a time-dependent manner, indicating the movement of the complexes from the lumen compartment to the hemolymph compartment. Upon the addition of BFA, a specific transcytosis inhibitor, decrease in fluorescence in the hemolymph was observed after 60 min compared to trials without inhibitors.[54] This is the first report that demonstrates the involvement of transcytosis in the translocation of dsRNA and nanoparticles through the midgut in lepidopterans. The ability of BAPCs to move within tissues via transcytosis is highly desirable for pest management, since it will allow for more widespread silencing effects.[12]

We also studied the endocytic uptake routes of the BAPC−dsRNA in Sf9 cells. Specific endocytosis inhibitors were used to individually target macropinocytosis, clathrin-mediated endocytosis, and caveolae-mediated endocytosis.[28,29] Confocal analysis indicated that macropinocytosis and clathrin-mediated endocytosis are the major uptake routes involved in BAPC−dsRNA complex internalization. Additionally, our results showed that once internalized, BAPC−dsRNA complexes are only minimally colocalized within lysosomes. This means they are able escape the endosomal pathway, possibly due to a phenomenon called the proton sponge effect. In this process, the endosomal membrane is destabilized by osmotic pressure because of a rapid influx of protons and solvated ions.[40] Endosomal escape is an important feature to consider toward the development of efficient dsRNA−biopesticides.[64]

Finally, exposure to BAPCs or BAPC−dsRNA complexes did not result in increased production of cytotoxic reactive nitrogen or oxygen species in Sf9 cells. Excess of either of these

https://doi.org/10.1021/acsomega.1c06638
ACS Omega 2022, 7, 10933−10943

cellular stress markers can indicate mitochondrial dysfunction, peroxisome activity, DNA damage, or cause lipid peroxidation and result in unwanted cell death to other off-target species.[57,61] The integrity of the cell membrane, which is essential for normal cell function was also maintained after exposing cells to BAPCs and the BAPC−dsRNA complexes. These findings are particularly relevant to ensure that BAPCs-based technology will not harm off-target species.

4. METHODS

4.1. Chemical Reagents and Cell Lines. Sf9 insect Cells (Novagen, St. Louis, MO, USA), sixth instar *S. frugiperda* (Benzon Research, Carlisle, PA, USA), 2,2,2-trifluoroethanol (TFE) (Thermo Fisher, USA), 6-well treated tissue culture plates (Corning Inc. Corning, NY, USA), 5(6)-carboxytetramethylrhodamine *N*-succinimidyl ester (Sigma-Aldrich, St. Louis, MO, USA), Grace's Insect Medium 1× supplemented (Thermo Fisher, USA), fetal bovine serum (FBS) (CPS Serum, Parkville, MO, USA), chlorpromazine (CPZ) (Sigma-Aldrich, St. Louis, MO, USA), dynasore and nystatin (Sigma-Aldrich, St. Louis, MO, USA), methyl-β-cyclodextrin (M-β-CD) (Millipore Sigma, USA), cytochalasin D (Cyt D) (Tocris Biosciences, MN, USA), brefeldin A (BFA) (Sigma-Aldrich, St. Louis, MO, USA), 7-aminoactinomycin D (7-AAD) (Tonbo, San Diego, CA), paraformaldehyde (Sigma-Aldrich, St. Louis, MO, USA), CYP450 dsRNA (RNA Greentech, USA), Griess reagent kit for nitrite quantification (Invitrogen, USA), CellROX Deep Red (Invitrogen, USA), and Cell Navigatior Lysosome Staining Kit—Green Fluorescence (AAT Bioquest, Sunnyvale, CA).

4.2. Synthesis of BAPCs. The peptides bis(Ac-FLIVI)$_2$−K−K$_4$−CONH$_2$ and bis(Ac-FLIVIGSII)$_2$−K−K$_4$−CONH$_2$ were synthesized as previously described.[4] To determine each peptide's concentration, they were separately dissolved in TFE and the absorbance of phenylalanine (two per sequence) at 257.5 nm was measured. In TFE, both peptides are helical and monomeric, thereby ensuring complete mixing when combined. After calculating concentrations, the peptides were then mixed at equimolar ratios to generate a stock with a calculated final concentration of 1 mM in the final volumes and then dried in vacuo. BAPCs were formed by hydrating dried peptides at 25 °C and allowed to stand for 10 min before solution was cooled and incubated at 4 °C for 1 h.[5] After 1 h, the peptide sample was returned to 25 °C for 30 min before drying for long-term storage or mixing with the dsRNA.

4.3. Preparation of Rhodamine-Labeled BAPCs (Rh−BAPCs). Rh−BAPCs were prepared similarly to the normal BAPCs, with slight variation. The bis(Ac-FLIVI)$_2$−K−K$_4$−CONH$_2$ component of the mixture was modified by the incorporation of N-hydroxysuccinimide ester of rhodamine B, and combined 1:1 with the unlabeled peptide (Method S1 and Figure S5) Thus, the final peptide mixture consisted of equimolar concentrations of bis(Ac-FLIVIGSII)$_2$−K−K$_4$−CONH$_2$ and bis(Ac-FLIVI)$_2$−K−K$_4$−CONH$_2$, with half of the latter being rhodamine labeled (25% Rh-labeled peptide and 75% unlabeled peptide). Work with Rh−BAPCs was performed protected from light to avoid quenching of the fluorophore. As previously described, the peptide mixture was then dissolved in nuclease-free water and incubated at room temperature for 10 min, then kept at 4 °C for 1 h. After 1 h, the peptide sample was returned to 25 °C for 30 min before drying for long-term storage or mixing with dsRNA. The biophysical characterization of the Rh−BAPCs was included in Figure S6 and Table S1.

4.4. Synthesis of dsRNA. The dsRNA sequences targeting the CYP-450 gene in *Popillia japonica* and *Spodoptera exigua* were designed and obtained from RNA Greentech LLC, Texas, USA. First, the mRNA sequence of CYP-450 (*P. japonica* GARJ01000597 and *S. exigua* KX443442.1) were obtained from NCBI nucleotide database. The selected gene sequences were further screened through GenScript siRNA target finder tool to predict siRNA sequences. The sequence region with highest predicted siRNAs was selected for dsRNA synthesis. Sequences from *S. frugiperda* were not selected for dsRNA design to allow testing for off-target effects. Nonetheless, the *S. exigua* CYP-450 sequence overlaps ∼90% with *S. frugiperda*. At least indicated, all experiments were carried out with the CYP-450 *P. japonica* gene.

4.5. Preparation of BAPC−dsRNA Complexes. To form the BAPC−dsRNA complexes, CYP-450 dsRNA (1 μg) suspended in nuclease-free water was added dropwise to aqueous solutions containing 50, 100, or 120 μM BAPCs or Rh−BAPCs. Solutions were then mixed carefully by pipet and allow to stand for 10 min before adding $CaCl_2$ (2.0 mM). The final solution was incubated another 30 min then used promptly for cellular uptake and transcytosis experiments. The biophysical characterization of the Rh−BAPC−dsRNA complexes was included in Figure S6 and Table S1.

4.6. Dynamic Light Scattering (DLS), Zeta Potential (ZP), and Transmission Electron Microscopy (TEM) Analysis. BAPC−dsRNA complexes were prepared following the protocol previously described. Particle sizes and zeta potentials of BAPCs and BAPC−dsRNA complexes were determined using a Zetasizer Nano ZS (Malvern Instruments Ltd., Westborough, MA). Samples were analyzed in nuclease-free water and all measurements were performed in triplicates. For TEM analysis, 50 μM of BAPCs mixed with or without 1 μg dsRNA were added directly onto individual grids (FCF 300-Cu, Formvar carbon film on a 300-mesh copper grid, Electron Microscopy Sciences, Hatfield, PA, USA) and allowed to dry for 2 h at room temperature. Next, samples were negatively stained using phosphotungstic acid and allowed to dry for additional 1 h. TEM imaging was performed at 60 kV on a Zeiss EM10.

4.7. Sf9 Cell Cultures and Growth Conditions. Sf9 cells were grown in supplemented Grace's Insect Media supplemented with 10% fetal bovine serum with no addition of antibiotics. Cell cultures were grown at 28 °C and ambient CO_2. Adherent cultures were passaged every fourth to fifth day by pipetting media gently across the growth surface until cells were homogeneously in solution. Cells were then transferred to a new T25 flask at 1 × 10^6 cells/mL. The media was replaced every 48 h or as needed.

4.8. Endocytosis Inhibition Study. Sf9 cells were seeded in 6-well plates containing glass coverslips at a concentration of 1 × 10^6 cells/mL and incubated for 36 h at 28 °C. Subsequently, media was removed, cells were washed with PBS and inhibitors of endocytosis were added in fresh media at their respective concentrations. Concentrations of inhibitors were as follows: M-β-CD at 5 mM, CPZ at 10 μM, dynasore at 80 μM, cytochalasin D at 4 μM, and nystatin at 50 μM. This inhibitor pretreatment was carried out for 30 min at 28 °C. After inhibitor pretreatment, Rh−BAPCs were added to the wells at a concentration of 50 μM and incubated for 1 h at 28 °C. Cells were washed once with PBS and then fixed for 15

https://doi.org/10.1021/acsomega.1c06638
ACS Omega 2022, 7, 10933−10943

min with 4% paraformaldehyde, followed by one more PBS wash. Coverslips were removed from the 6-well plates and mounted to microscope slides using ProLong Diamond Antifade Mountant. Fluorescent imaging was carried out using the Nikon A1R MP Confocal Microscope. The same protocol was used for endocytic analysis of BAPC−dsRNA complexes with Rh−BAPCs being conjugated with dsRNA.

4.9. Determination of Reactive Nitrogen Species (RNS) and Reactive Oxygen Species (ROS). Reactive nitrogen (nitric oxide) species were detected using the Griess Reagent Kit for Nitrite Determination from Invitrogen. Cells were seeded in 96-well plates at a concentration of 1×10^6 and incubated for 48 h at 28 °C. Cell media was removed, and cells were washed with PBS. After inhibitor pretreatment, BAPCs or BAPC−dsRNA complexes were added to the wells at a concentration of 50, 100, and 120 μM and incubated for 1 h at 28 °C. Cells were then treated with the Griess reagent as per kit instructions. A standard curve was created by diluting the provided nitrite solutions to final concentrations of 0, 1, 5, 10, 20, 30, 40, and 50 μM. Absorbance at 548 nm was read using automatic plate reader BioTek Cytation3.

The presence of ROS was detected using CellROX Deep Red Reagent. Cells were seeded in 96-well plates containing glass coverslips at a concentration of 1×10^6 and incubated for 48 h at 28 °C. Media was removed, cells were washed with PBS, and inhibitors of endocytosis were added in fresh media at their respective concentrations, listed previously. Inhibitor pretreatment was carried out for 30 min at 28 °C. After inhibitor pretreatment, BAPCs or BAPC−dsRNA complexes were added to the wells at a concentration of 50, 100, and 120 μM and incubated for 1 h at 28 °C. Subsequently, cells were incubated with CellROX Deep Red Reagent (640/655 nm) at a final concentration of 5 μM and protected from light for 30 min at 28 °C. Fluorescence was read at 655 nm.

4.10. Cytotoxicity Experiment Using Flow Cytometry. Sf9 cells were seeded in 12-well plates at a concentration of 1×10^6 cells/mL and incubated for 36 h at 28 °C. Cell media was then removed, and media with BAPCs or BAPC−dsRNA complexes at 50, 100, or 120 μM were added into the appropriate wells at the concentration previously listed. Same protocol was followed for the endocytosis inhibitors, using the concentrations previously listed. The plates were then incubated for 30 min at 28 °C. Cells were incubated an additional hour; then, they were washed with PBS and detached from the wells by pipetting. After centrifugation at 1700 rpm for 5 min, cells were resuspended in PBS and 7-AAD was added to detect and exclude dead cells. A total of 10 000 events per sample were analyzed using a MACSQuant Analyzer 10, Miltenyi Biotec. Side scatter vs forward scatter gating method was used to eliminate debris and cell clumps. A full gating strategy is shown in Figure S7. Data was analyzed using FlowLogic (Miltenyi Biotec) software.

4.11. Lysosome Colocalization. Cells were seeded in a 6-well plate containing sterile glass coverslips at 1×10^6 cells/mL and incubated for 36 h at 28 °C. Cell media was removed, and cells were washed with PBS. The working solution of Cell Navigator was prepared as according to kit instructions. A 1:1 ratio of cell media to Cell Navigator solution was added to the wells, and cells were incubated 2 h at 28 °C. Rh−BAPCs (50 μM) complexed with dsRNA (1 μg) were added into the wells 30 min before the Cell Navigator solution was removed. Cells were, then, washed with PBS twice, and coverslips were mounted using ProLong Diamond Antifade Mountant (Thermo) and allowed to dry overnight protected from light overnight. Slides were then imaged using the Nikon A1R Confocal Microscope.

4.12. Insect Rearing. *S. frugiperda* (fall armyworm) eggs placed in individual growth containers were obtained from Benzon Research (Carlisle, PA, USA). Larvae were reared on a provided wheat germ and soy flour-based artificial diet in a growth chamber at 29 °C with a 12:12 (L:D) photoperiod. Larvae were grown until reaching sixth instar and then were selected for Ussing chamber experiments.

4.13. Midgut Isolation. Larvae were selected after reaching sixth instar but before pupation for dissection. Dissections were performed in insect physiological solution (47 mmol/L KCl, 20.5 mmol/L $MgCl_2$, 20 mmol/L $MgSO_4$, 1 mmol/L $CaCl_2$, 88 mmol/L sucrose, 4.3 mmol/L K_2HPO_4, 1.1 mmol/L KH_2PO_4, adjusted to pH 7.5) at room temperature.[12] The midgut was exposed by creating a longitudinal incision on the ventrolateral side. The midgut was isolated and stabilized between two pins before opening it longitudinally. The procedure was done carefully to avoid puncturing, as perforation of the midgut will result in diffusion of particles between chambers rather than active transport. Once opened, the gut was rinsed with insect physiological solution to remove debris then immediately mounted on a modified 0.1 cm^2 slider (Figure S8A) with great care to conserve lumenal and hemolymphatic orientation.

4.14. Ex Vivo Transcytosis Experiments. Midguts mounted in sliders were inserted into an Ussing chamber (Physiologic Instruments, San Diego, CA, USA; Model P2300) (Figure S8B). The tissue was perfused with 2−3 mL lumenal buffer (5 mmol/L CaCl2, 24 mmol/L $MgSO_4$, 20 mmol/L potassium gluconate, 190 mmol/L sucrose, 5 mmol/L CAPS, pH 10.0) on the lumen side of the midgut, and 2−3 mL of hemolymph buffer (5 mmol/L CaCl2, 24 mmol/L MgSO4, 20 mmol/L potassium gluconate, 190 mmol/L sucrose, 5 mmol/L Tris, pH 7.0) on the hemolymphatic side. Air was bubbled gently to each side of the tissue using a Tetra Whisper Air Pump (30−60 gallons; Tetra, Blacksburg, VA, USA). Air flow rate used was 2.6L/min. Experiments were run at 25 °C protected from light. Rh−BAPCs (50 μM) and Rh−BAPC−dsRNA (50 μM + 1 μg dsRNA) complexes were added to the lumenal buffer and 100 μL samples were taken at 0, 15, 30, and, 60 min from both sides. Transcytosis-specific inhibitor BFA (10 μM) and endocytosis inhibitor CPZ (10 μM) was added 30 min prior to adding BAPCs or complexes. Samples were loaded in a dark-sided 96-well plate and analyzed using a BioTek Cytation 3 plate reader (excitation 544 nm, emission 576 nm). Change in relative fluorescence over time was plotted to visualize the subsequent fluctuation of relative fluorescence because of transcytosis. dsRNA-CYP-450 (*S. exigua*) was used for this set of experiments.

4.15. Confocal Laser Scanning Microscopy. Images were obtained using a Nikon A1R MP confocal microscope (Carl Zeiss, Gottingen, Germany).

4.16. Software and Statistical Analyses. Statistics were performed using GraphPad Prism 5 software (GraphPad Software, La Jolla, CA). A minimum of two replicates were performed for all conditions. Figures were created using biorender.com and Adobe Photoshop CC 2019.

https://doi.org/10.1021/acsomega.1c06638
ACS Omega 2022, 7, 10933−10943

■ ASSOCIATED CONTENT

Supporting Information

The Supporting Information is available free of charge at https://pubs.acs.org/doi/10.1021/acsomega.1c06638.

Detailed protocol for the synthesis of the rhodamine-labeled peptide bis(Ac-FLIVI)$_2$−K−K$_4$−CONH$_2$; size distribution of BAPCs (50 μM) associated with dsRNA (1 μg); DLS and ZP of Rh−BAPCs and Rh−BAPCs−dsRNA complexes; additional inhibitors used in the inhibition assay of BAPCs and BAPC−dsRNA complexes in Sf9 cells; transcytosis of Rh−BAPCs through *S. frugiperda* midgut in the presence of transcytosis and endocytosis inhibitors; SF9 cell viability assay with different endocytosis inhibitors; RP-HPLC and MS analysis of the rhodamine-labeled peptide bis(Ac-FLIVI)$_2$−K−K$_4$−CONH$_2$; TEM characterization Rh−BAPCs and Rh−BAPCs−dsRNA complexes; flow cytometry gating strategy for cell viability studies; and Ussing chamber setup (PDF)

■ AUTHOR INFORMATION

Corresponding Author

L. Adriana Avila − *Department of Biological Sciences, Auburn University, Auburn, Alabama 36849-5412, United States;* orcid.org/0000-0001-6788-6975; Phone: +334-844-1659; Email: adriana.avila@auburn.edu

Authors

Erin McGraw − *Department of Biological Sciences, Auburn University, Auburn, Alabama 36849-5412, United States;* orcid.org/0000-0002-5162-8004

Jonathan D. Roberts − *Department of Biological Sciences, Auburn University, Auburn, Alabama 36849-5412, United States;* Present Address: Alabama College of Osteopathic Medicine, Dothan, AL, USA

Nitish Kunte − *Department of Biological Sciences, Auburn University, Auburn, Alabama 36849-5412, United States;* orcid.org/0000-0002-6429-6125

Matthew Westerfield − *Department of Biological Sciences, Auburn University, Auburn, Alabama 36849-5412, United States*

Xavier Streety − *Department of Biological Sciences, Auburn University, Auburn, Alabama 36849-5412, United States;* Present Address: Department of Chemistry, Vanderbilt University, Nashville, TN, USA

David Held − *Department of Entomology and Plant Pathology, Auburn University, Auburn, Alabama 36849-5412, United States*

Complete contact information is available at: https://pubs.acs.org/10.1021/acsomega.1c06638

Author Contributions

†E.M. and J.D.R. made equal contributions.

Notes

The authors declare no competing financial interest.

■ ACKNOWLEDGMENTS

This project was supported by the Alabama Agricultural Experiment Station and the Hatch program of the National Institute of Food and Agriculture, U.S. Department of Agriculture. We would also like to thank the lab of Dr. John Tomich at Kansas State University for supplying the rhodamine labelled peptide used in this work.

■ REFERENCES

(1) Zhu, K. Y.; Palli, S. R. Mechanisms, Applications, and Challenges of Insect RNA Interference. *Annual Review of Entomology* **2020**, *65*, 293−311.

(2) Kunte, N.; McGraw, E.; Bell, S.; Held, D.; Avila, L.-A. Prospects, Challenges and Current Status of RNAi through Insect Feeding. *Pest Manag. Sci.* **2020**, *76*, 26−41.

(3) Zhang, H.; Li, H.-C.; Miao, X.-X. Feasibility, Limitation and Possible Solutions of RNAi-Based Technology for Insect Pest Control. *Insect Sci.* **2013**, *20*, 15−30.

(4) Sukthankar, P.; Avila, L. A.; Whitaker, S. K.; Iwamoto, T.; Morgenstern, A.; Apostolidis, C.; Liu, K.; Hanzlik, R. P.; Dadachova, E.; Tomich, J. M. Branched Amphiphilic Peptide Capsules: Cellular Uptake and Retention of Encapsulated Solutes. *Biochim. Biophys. Acta - Biomembr.* **2014**, *1838*, 2296−2305.

(5) Avila, L. A.; Aps, L. R. M. M.; Ploscariu, N.; Sukthankar, P.; Guo, R.; Wilkinson, K. E.; Games, P.; Szoszkiewicz, R.; Alves, R. P. S.; Diniz, M. O.; et al. Gene Delivery and Immunomodulatory Effects of Plasmid DNA Associated with Branched Amphiphilic Peptide Capsules. *J. Controlled Release* **2016**, *241*, 15−24.

(6) Avila, L. A.; Chandrasekar, R.; Wilkinson, K. E.; Balthazor, J.; Heerman, M.; Bechard, J.; Brown, S.; Park, Y.; Dhar, S.; Reeck, G. R.; Tomich, J. M. Delivery of Lethal DsRNAs in Insect Diets by Branched Amphiphilic Peptide Capsules. *J. Controlled Release* **2018**, *273*, 139−146.

(7) Barros, S. de M.; Whitaker, S. K.; Sukthankar, P.; Avila, L. A.; Gudlur, S.; Warner, M.; Beltrão, E. I. C. C.; Tomich, J. M. A Review of Solute Encapsulating Nanoparticles Used as Delivery Systems with Emphasis on Branched Amphipathic Peptide Capsules. *Arch. Biochem. Biophys.* **2016**, *596*, 22−42.

(8) Jarvis, D. L.; Oker-Blom, C.; Summers, M. D. Role of Glycosylation in the Transport of Recombinant Glycoproteins through the Secretory Pathway of Lepidopteran Insect Cells. *J. Cell. Biochem.* **1990**, *42*, 181−191.

(9) Bernales, S.; Papa, F. R.; Walter, P. Intracellular Signaling by the Unfolded Protein Response. *Annu. Rev. Cell Dev. Biol.* **2006**, *22*, 487−508.

(10) White, L. D.; Coates, C. J.; Atkinson, P. W.; O'Brochta, D. A. An Eye Color Gene for the Detection of Transgenic Non-Drosophilid Insects. *Insect Biochem. Mol. Biol.* **1996**, *26*, 641−644.

(11) Sijen, T.; Fleenor, J.; Simmer, F.; Thijssen, K. L.; Parrish, S.; Timmons, L.; Plasterk, R. H. A.; Fire, A. On the Role of RNA Amplification in DsRNA-Triggered Gene Silencing. *Cell* **2001**, *107*, 465−476.

(12) Kemmerer, M.; Bonning, B. C. Transcytosis of Junonia Coenia Densovirus VP4 across the Gut Epithelium of Spodoptera Frugiperda (Lepidoptera: Noctuidae). *Insect Sci.* **2020**, *27*, 22−32.

(13) Ussing, H. H.; Zerahn, K. Active Transport of Sodium as the Source of Electric Current in the Short-Circuited Isolated Frog Skin. *Acta Physiol. Scand.* **1951**, *23*, 110−127.

(14) Granados, R. R.; Li, G.; Blissard, G. W. Insect Cell Culture and Biotechnology. *Virol. Sin.* **2007**, *22*, 83−93.

(15) Sahay, G.; Alakhova, D. Y.; Kabanov, A. V. Endocytosis of Nanomedicines. *J. Controlled Release* **2010**, *145*, 182−195.

(16) Vélez, A. M.; Fishilevich, E. The Mysteries of Insect RNAi: A Focus on DsRNA Uptake and Transport. *Pestic. Biochem. Physiol.* **2018**, *151*, 25−31.

(17) Yoon, J. S.; Gurusamy, D.; Palli, S. R. Accumulation of DsRNA in Endosomes Contributes to Inefficient RNA Interference in the Fall Armyworm, Spodoptera Frugiperda. *Insect Biochem. Mol. Biol.* **2017**, *90*, 53−60.

(18) Patel, S.; Kim, J.; Herrera, M.; Mukherjee, A.; Kabanov, A. V.; Sahay, G. Brief Update on Endocytosis of Nanomedicines. *Adv. Drug Delivery Rev.* **2019**, *144*, 90−111.

(19) Simovic, S.; Song, Y.; Nann, T.; Desai, T. A. Intestinal Absorption of Fluorescently Labeled Nanoparticles. *Nanomedicine Nanotechnology, Biol. Med.* **2015**, *11*, 1169−1178.
(20) Gilleron, J.; Querbes, W.; Zeigerer, A.; Borodovsky, A.; Marsico, G.; Schubert, U.; Manygoats, K.; Seifert, S.; Andree, C.; Stöter, M.; et al. Image-Based Analysis of Lipid Nanoparticle-Mediated SiRNA Delivery, Intracellular Trafficking and Endosomal Escape. *Nat. Biotechnol.* **2013**, *31*, 638−646.
(21) Avila, L. A.; Aps, L. R. M. M.; Sukthankar, P.; Ploscariu, N.; Gudlur, S.; Šimo, L.; Szoszkiewicz, R.; Park, Y.; Lee, S. Y.; Iwamoto, T.; Ferreira, L. C. S.; Tomich, J. M. Branched Amphiphilic Cationic Oligopeptides Form Peptiplexes with DNA: A Study of Their Biophysical Properties and Transfection Efficiency. *Mol. Pharmaceutics* **2015**, *12*, 706−715.
(22) Ramos, A. P. Dynamic Light Scattering Applied to Nanoparticle Characterization. In *Nanocharacterization Techniques;* Da Roz, A. L., Ferreira, M., de Lima Leite, F., Oliveria, O. N., Eds.; William Andrew Publishing, 2017; pp 99−110.
(23) Maguire, C. M.; Rösslein, M.; Wick, P.; Prina-Mello, A. Characterisation of Particles in Solution−a Perspective on Light Scattering and Comparative Technologies. *Sci. Technol. Adv. Mater.* **2018**, *19*, 732−745.
(24) Bhattacharjee, S. DLS and Zeta Potential - What They Are and What They Are Not? *J. Controlled Release* **2016**, *235*, 337−351.
(25) Shao, X. R.; Wei, X. Q.; Song, X.; Hao, L. Y.; Cai, X. X.; Zhang, Z. R.; Peng, Q.; Lin, Y. F. Independent Effect of Polymeric Nanoparticle Zeta Potential/Surface Charge, on Their Cytotoxicity and Affinity to Cells. *Cell Prolif* **2015**, *48*, 465−474.
(26) Gumustas, M.; Sengel-Turk, C. T.; Gumustas, A.; Ozkan, S. A.; Uslu, B. Effect of Polymer-Based Nanoparticles on the Assay of Antimicrobial Drug Delivery Systems. In *Multifunctional Systems for Combined Delivery, Biosensing and Diagnostics*; Grumezescu, A. M., Ed.; Elsevier, 2017; pp 67−108.
(27) Natarajan, P.; Roberts, J. D.; Kunte, N.; Hunter, W. B.; Fleming, S. D.; Tomich, J. M.; Avila, L. A. A Study of the Cellular Uptake of Magnetic Branched Amphiphilic Peptide Capsules. *Mol. Pharmaceutics* **2020**, *17*, 2208−2220.
(28) Vercauteren, D.; Vandenbroucke, R. E.; Jones, A. T.; Rejman, J.; Demeester, J.; De Smedt, S. C.; Sanders, N. N.; Braeckmans, K. The Use of Inhibitors to Study Endocytic Pathways of Gene Carriers: Optimization and Pitfalls. *Mol. Ther.* **2010**, *18*, 561−569.
(29) Dutta, D.; Donaldson, J. G. Search for Inhibitors of Endocytosis. *Cell. Logist.* **2012**, *2*, 203−208.
(30) Sato, K.; Nagai, J.; Mitsui, N.; Yumoto, R.; Takano, M. Effects of Endocytosis Inhibitors on Internalization of Human IgG by Caco-2 Human Intestinal Epithelial Cells. *Life Sci.* **2009**, *85*, 800−807.
(31) Saha, K.; Kim, S. T.; Yan, B.; Miranda, O. R.; Alfonso, F. S.; Shlosman, D.; Rotello, V. M. Surface Functionality of Nanoparticles Determines Cellular Uptake Mechanisms in Mammalian Cells. *Small* **2013**, *9*, 300−305.
(32) Hillaireau, H.; Couvreur, P. Nanocarriers' Entry into the Cell: Relevance to Drug Delivery. *Cell. Mol. Life Sci.* **2009**, *66*, 2873−2896.
(33) Date, A. A.; Hanes, J.; Ensign, L. M. Nanoparticles for Oral Delivery: Design, Evaluation and State-of-the-Art. *J. Controlled Release* **2016**, *240*, 504−526.
(34) Hodgson, J. J.; Buchon, N.; Blissard, G. W. Identification of Insect Genes Involved in Baculovirus AcMNPV Entry into Insect Cells. *Virology* **2019**, *527*, 1−11.
(35) Van Hoof, D.; Rodenburg, K. W.; Van Der Horst, D. J. Receptor-Mediated Endocytosis and Intracellular Trafficking of Lipoproteins and Transferrin in Insect Cells. *Insect Biochem. Mol. Biol.* **2005**, *35*, 117−128.
(36) Long, G.; Pan, X.; Kormelink, R.; Vlak, J. M. Functional Entry of Baculovirus into Insect and Mammalian Cells Is Dependent on Clathrin-Mediated Endocytosis. *J. Virol.* **2006**, *80*, 8830−8833.
(37) Kunz, D.; Oliveira, G. B.; Uchôa, A. F.; Samuels, R. I.; Macedo, M. L. R.; Silva, C. P. Receptor Mediated Endocytosis of Vicilin in Callosobruchus Maculatus (Coleoptera: Chrysomelidae) Larval Midgut Epithelial Cells. *Comp. Biochem. Physiol. Part - B Biochem. Mol. Biol.* **2017**, *210*, 39−47.
(38) Mercer, J.; Helenius, A. Virus Entry by Macropinocytosis. *Nat. Cell Biol.* **2009**, *11*, 510−520.
(39) Paillard, A.; Hindré, F.; Vignes-Colombeix, C.; Benoit, J. P.; Garcion, E. The Importance of Endo-Lysosomal Escape with Lipid Nanocapsules for Drug Subcellular Bioavailability. *Biomaterials* **2010**, *31*, 7542−7554.
(40) Ballabio, A. The Awesome Lysosome. *EMBO Mol. Med.* **2016**, *8*, 73−76.
(41) Battistella, C.; Klok, H. A. Controlling and Monitoring Intracellular Delivery of Anticancer Polymer Nanomedicines. *Macromol. Biosci.* **2017**, *17*, 1700022.
(42) Meng, Z.; Luan, L.; Kang, Z.; Feng, S.; Meng, Q.; Liu, K. Histidine-Enriched Multifunctional Peptide Vectors with Enhanced Cellular Uptake and Endosomal Escape for Gene Delivery. *J. Mater. Chem. B* **2017**, *5*, 74−84.
(43) Shete, H. K.; Prabhu, R. H.; Patravale, V. B. Endosomal Escape: A Bottleneck in Intracellular Delivery. *J. Nanosci. Nanotechnol.* **2014**, *14*, 460−474.
(44) Saadat, M.; Zahednezhad, F.; Zakeri-Milani, P.; Reza Heidari, H.; Shahbazi-Mojarrad, J.; Valizadeh, H. Drug Targeting Strategies Based on Charge Dependent Uptake of Nanoparticles into Cancer Cells. *J. Pharm. Pharm. Sci.* **2019**, *22*, 191−220.
(45) Freeman, E. C.; Weiland, L. M.; Meng, W. S. Modeling the Proton Sponge Hypothesis: Examining Proton Sponge Effectiveness for Enhancing Intracellular Gene Delivery through Multiscale Modeling. *J. Biomater. Sci. Polym. Ed.* **2013**, *24*, 398−416.
(46) Shukla, J. N.; Kalsi, M.; Sethi, A.; Narva, K. E.; Fishilevich, E.; Singh, S.; Mogilicherla, K.; Palli, S. R. Reduced Stability and Intracellular Transport of DsRNA Contribute to Poor RNAi Response in Lepidopteran Insects. *RNA Biol.* **2016**, *13*, 656−669.
(47) Funhoff, A. M.; van Nostrum, C. F.; Koning, G. A.; Schuurmans-Nieuwenbroek, N. M. E.; Crommelin, D. J. A.; Hennink, W. E. Endosomal Escape of Polymeric Gene Delivery Complexes Is Not Always Enhanced by Polymers Buffering at Low PH. *Biomacromolecules* **2004**, *5*, 32−39.
(48) Denecke, S.; Swevers, L.; Douris, V.; Vontas, J. How Do Oral Insecticidal Compounds Cross the Insect Midgut Epithelium? *Insect Biochem. Mol. Biol.* **2018**, *103*, 22−35.
(49) Aronstein, K.; Pankiw, T.; Saldivar, E. SID-I Is Implicated in Systemic Gene Silencing in the Honey Bee. *J. Apic. Res.* **2006**, *45*, 20−24.
(50) Cappelle, K.; De Oliveira, C. F. R.; Van Eynde, B.; Christiaens, O.; Smagghe, G. The Involvement of Clathrin-Mediated Endocytosis and Two Sid-1-like Transmembrane Proteins in Double-Stranded RNA Uptake in the Colorado Potato Beetle Midgut. *Insect Mol. Biol.* **2016**, *25*, 315−323.
(51) Luo, Y.; Wang, X.; Yu, D.; Kang, L. The SID-1 Double-Stranded RNA Transporter Is Not Required for Systemic RNAi in the Migratory Locust. *RNA Biol.* **2012**, *9*, 663−671.
(52) Tuma, P. L.; Hubbard, A. L. Transcytosis: Crossing Cellular Barriers. *Physiol. Rev.* **2003**, *83*, 871−932.
(53) Gibco. *Growth and Maintenance of Insect Cell Lines: User Guide*; ThermoFisher Scientific, 2017. https://tools.thermofisher.com/content/sfs/manuals/Insect_Cell_Lines_UG.pdf
(54) Hunziker, W.; Andrew Whitney, J.; Mellman, I. Selective Inhibition of Transcytosis by Brefeldin A in MDCK Cells. *Cell* **1991**, *67*, 617−627.
(55) Kaksonen, M.; Roux, A. Mechanisms of Clathrin-Mediated Endocytosis. *Nat. Rev. Mol. Cell Biol.* **2018**, *19*, 313−326.
(56) Roger, E.; Lagarce, F.; Garcion, E.; Benoit, J. P. Lipid Nanocarriers Improve Paclitaxel Transport throughout Human Intestinal Epithelial Cells by Using Vesicle-Mediated Transcytosis. *J. Controlled Release* **2009**, *140*, 174−181.
(57) Manke, A.; Wang, L.; Rojanasakul, Y. Mechanisms of Nanoparticle-Induced Oxidative Stress and Toxicity. *BioMed. Research International* **2013**, *2013*, 1.

https://doi.org/10.1021/acsomega.1c06638
ACS Omega 2022, 7, 10933−10943

(58) Yu, Z.; Li, Q.; Wang, J.; Yu, Y.; Wang, Y.; Zhou, Q.; Li, P. Reactive Oxygen Species-Related Nanoparticle Toxicity in the Biomedical Field. *Nanoscale Res. Lett.* **2020**, DOI: 10.1186/s11671-020-03344-7.
(59) Ansari, M. O.; Parveen, N.; Ahmad, M. F.; Wani, A. L.; Afrin, S.; Rahman, Y.; Jameel, S.; Khan, Y. A.; Siddique, H. R.; Tabish, M.; Shadab, G. G. H. A. Evaluation of DNA Interaction, Genotoxicity and Oxidative Stress Induced by Iron Oxide Nanoparticles Both in Vitro and in Vivo: Attenuation by Thymoquinone. *Sci. Rep.* **2019**, *9*, 6912.
(60) Patlolla, A. K.; Shinde, A. K.; Tchounwou, P. B. A Comparison of Poly-Ethylene-Glycol-Coated and Uncoated Gold Nanoparticle-Mediated Hepatotoxicity and Oxidative Stress in Sprague Dawley Rats. *Int. J. Nanomedicine* **2019**, *14*, 639−647.
(61) Di Meo, S.; Reed, T. T.; Venditti, P.; Victor, V. M. Role of ROS and RNS Sources in Physiological and Pathological Conditions. *Oxidative Medicine and Cellular Longevity* **2016**, *2016*, 1.
(62) Hardy, M.; Zielonka, J.; Karoui, H.; Sikora, A.; Michalski, R.; Podsiadły, R.; Lopez, M.; Vasquez-Vivar, J.; Kalyanaraman, B.; Ouari, O. Detection and Characterization of Reactive Oxygen and Nitrogen Species in Biological Systems by Monitoring Species-Specific Products. *Antioxidants and Redox Signaling* **2018**, *28*, 1416−1432.
(63) McGraw, E.; Dissanayaka, R. H. R.; Vaughan, J. J. C.; Kunte, N.; Mills, G.; Laurent, G. M. G. G. M.; Avila, L. A. A. Laser-Assisted Delivery of Molecules in Fungal Cells. *ACS Appl. Bio Mater.* **2020**, *3*, 6167−6176.
(64) Gurusamy, D.; Mogilicherla, K.; Shukla, J. N.; Palli, S. R. Lipids Help Double-Stranded RNA in Endosomal Escape and Improve RNA Interference in the Fall Armyworm, *Spodoptera frugiperda*. *Arch. Insect Biochem. Physiol.* **2020**, DOI: 10.1002/arch.21678.

https://doi.org/10.1021/acsomega.1c06638
ACS Omega 2022, 7, 10933−10943